Int. J. Heat Mass Transfer. Vol. 29, No. 11, pp. 1655–1667, 1986
Printed in Great Britain

0017–9310/86 $3.00 + 0.00
Pergamon Journals Ltd.

Multiple steady-state solutions for horizontal buoyant flows in cold water

IBRAHIM EL-HENAWY,* BENJAMIN GEBHART†
and NICHOLAS D. KAZARINOFF‡

* Department of Mathematics, Mansoora University, Mansoora, Egypt
† Mechanical Engineering and Applied Mechanics, University of Pennsylvania, Philadelphia, PA 19104, U.S.A.
‡ Department of Mathematics, Diefendorf Hall, SUNY/B, Buffalo, NY 14214, U.S.A.

(*Received* 10 *October* 1985 *and in final form* 19 *February* 1986)

Abstract—The buoyancy force arising from temperature gradients in cold water is bidirectional if the temperature range spans that of the density extremum. Many large scale and subtle consequences of this are now known, for some of the most common flow configurations. The first calculations for horizontal flows encountered a wide range of conditions for which boundary-layer solutions were not obtained. Results here narrow that range considerably. They also accurately determine the residual gap of no solutions, in terms of a density extremum parameter R. Of equal interest, these calculations have found multiple solutions over ranges of R, on each side of the gap. In some regions, the properties of the second set of solutions are very different and unusual, among buoyancy induced flows. Very weak flows are found which, nevertheless, may be very unstable. Extremely low heat transfer rates arise under some conditions.

INTRODUCTION

THE HEAT transfer and flows arising from buoyant fluids adjacent to horizontal or nearly horizontal surfaces have not been studied as extensively as those adjacent to vertical surfaces and in freely rising plumes. However, these flows arise in many applications, both in the environment and in technology. The flows of concern here are those adjacent to a horizontal surface, in an extensive ambient medium, as a result of a surface temperature different from that of the ambient medium. Past observations of flows arising from isolated surfaces have shown the existence, close to the surface, of a boundary-layer mode of convection, followed, after a region of instability, by a cellular motion. Schmidt [1] was apparently the first to investigate experimentally flow above a flat, horizontal surface.

With only thermal buoyancy effects, and the usual approximations concerning density levels and differences, often called the Boussinesq or conventional approximations, Stewartson [2] analyzed transport adjacent to a semi-infinite isothermal surface. The flow was assumed to arise downstream from a single leading edge. Gill *et al.* [3] later showed that the necessary condition for such flows was that the buoyancy force be away from the surface, as for a heated surface facing upward or a cooled surface facing downward.

Rotem and Claassen [4, 5] obtained solutions for an isothermal horizontal surface for several specific values of the Prandtl number. Asymptotic results for zero and infinite Prandtl numbers are also given in ref. [4]. Experimental observations with a schlieren system clearly indicated the existence of a boundary layer near the leading edge on the upper side of a heated horizontal surface, insulated on the bottom face. Rotem [6] and Rotem and Claassen [4] also formulated the similarity solution for horizontal axisymmetric boundary-layer flow adjacent to an unbounded horizontal surface and gave solutions for an isothermal surface condition for an unspecified Prandtl number. These are sometimes called disk flows, in contrast to the plane flows previously considered.

Pera and Gebhart [7, 8] studied both flow and the stability of horizontal and slightly inclined plane flows. For a horizontal orientation, the experimental results in air indicated an attached region, with characteristics close to those predicted. This region was followed downstream by a flow separation in the form of very rapidly growing longitudinal vortices. This latter consequence, along with upstream disturbance growth characteristics, implied an initiating role for upstream two-dimensional spanwise disturbances.

For the disk flows studied in refs. [4, 6], Blanc and Gebhart [9] discuss the limits of physical reasonableness of a downstream variation of $t_0 - t_\infty$, i.e. the difference between the local surface and ambient medium temperatures. Solutions are given for both isothermal and uniform flux conditions, for t_∞ uniform. Then procedures are presented which give exact solutions of some disk and plane flows.

The present paper treats horizontal plane flows, generated in both pure and saline water, at temperature conditions which may result in density extrema in the convection region, e.g. at about 4°C at a pressure of 1 bar in pure water. Such flows are found in the melting and freezing of ice surfaces and in processing technology.

NOMENCLATURE

a, b, c	defined in equations (9), (17) and (18)
B	buoyancy force, $g(\rho_\infty - \rho)$
c_p	specific heat of water
f	nondimensional streamfunction
G	modified Grashof number, $5(Gr_x/5)^{1/5}$
Gr_x	Grashof number
g	acceleration due to gravity
k	thermal conductivity
P	nondimensional motion pressure
Pr	Prandtl number
p_m	motion pressure
q	exponent in density equation (2)
R	$(t_m - t_\infty)/(t_0 - t_\infty)$
s	salinity
t	temperature
t_m	temperature where the density is maximum
t_0	surface temperature
t_∞	ambient temperature
u	tangential velocity component
v	normal velocity component
W	nondimensional local buoyancy force
x	distance along the surface
y	distance normal to the surface.

Greek symbols

α	coefficient in density equation (2)
β	coefficient of thermal expansion
η	nondimensional distance in the boundary region
η_∞	value of η at the outside edge of the region of calculation
ν	kinematic viscosity
ρ	density
ρ_m	maximum density
ρ_∞	density of ambient fluid
ϕ	nondimensional temperature, $(t - t_\infty)/(t_0 - t_\infty)$
ψ	streamfunction.

Superscript

′	differentiation with respect to η.

These were first studied by Gebhart *et al.* [10], for both plane and disk flows, using a formulation for transport similar to that given by Gebhart and Mollendorf [11] for vertical flows. Buoyancy-driven transport may be, relatively, very complicated when the imposed temperature conditions, t_0 and t_∞, are low, in the region of the density extremum, at t_m. If t_0 and t_∞ span t_m, a buoyancy force reversal arises across the thermal layer, all the way downstream in the fluid. If this is sufficiently severe, flow reversal may be generated across the transport region. This tendency, in turn, may lead to complete reversal of the overall flow patterns. This is called convective inversion.

These effects, in terms of the local buoyancy force, $B = g(\rho_\infty - \rho)$ are depicted in Fig. 1. The density vs temperature variation sketched in Fig. 1(a) shows four typical choices (1, 2, 3 and 4) of the imposed temperature conditions t_0 and t_∞, in relation to the temperature at the extremum, t_m. These three temperatures are related as follows:

$$R = \frac{t_m(s,p) - t_\infty}{t_0 - t_\infty}. \quad (1)$$

The four choices in Fig. 1 represent the four regimes of buoyancy force variation, $B = g(\rho_\infty - \rho)$, which arise with an extremum. These regimes are shown, over the range of R in Fig. 1(b). For choice 1, B is everywhere upward, or positive, across the thermal region and $R < 0$. For 2, B is everywhere downward. This condition persists for all larger values of $t_{0,2}$ until $\rho(t_{0,2}) = \rho(t_{\infty,2})$, for a symmetric density variation. This is the region $R \geqslant 1/2$. For 3, the buoyancy force is upward near the surface, with an outside region of buoyancy force reversal, to downward. This is the range of R just above $R = 0$. For choice 4, B is downward near the surface and upward further out. This is the region below $R = 1/2$. Intermediate in the range $0 < R < 1/2$, the opposing effects are comparable. For choices 3 and 4, local flow reversals arise. Then the net flow direction is unclear. It is in this region that a gap arises in solutions of the boundary layer formulation.

The calculations of Gebhart and Mollendorf [11], for flows adjacent to vertical isothermal surfaces, cover the ranges of unidirectional buoyancy force, that is, outside of $0 < R < 1/2$. Both pure and saline water were considered.

The formulation of the local buoyancy force, $B = g(\rho_\infty - \rho)$, used the very simple, yet very accurate, density relation for pure and saline water developed by Gebhart and Mollendorf [12], given below in equation (2). It applies to water in the range of $t = 0$ to 20°C, salinity $s = 0$ to 40 p.p.t. and pressure p to 1000 bar. The agreement with the most modern density data over this whole region is about 9 p.p.m. (r.m.s.). The agreement with other modern pure water results is 3.5 p.p.m. (r.m.s.). The relation is

$$\rho(t,s,p) = \rho_m(s,p)\,[1 - \alpha(s,p)\,|t - t_m(s,p)|^{q(s,p)}] \quad (2)$$

where $\rho_m(s,p)$ is the maximum density at s and p, $t_m(s,p)$ is the corresponding inversion temperature at maximum density and $q(s,p)$ is the exponent. For pure water at 1 bar, $q = 1.894816$, $\alpha = 9.297173 \times 10^{-6}$ $(°C)^{-q}$ and $t_m = 4.029325$°C. Equation (2) contains only a single term in temperature. This simplicity is

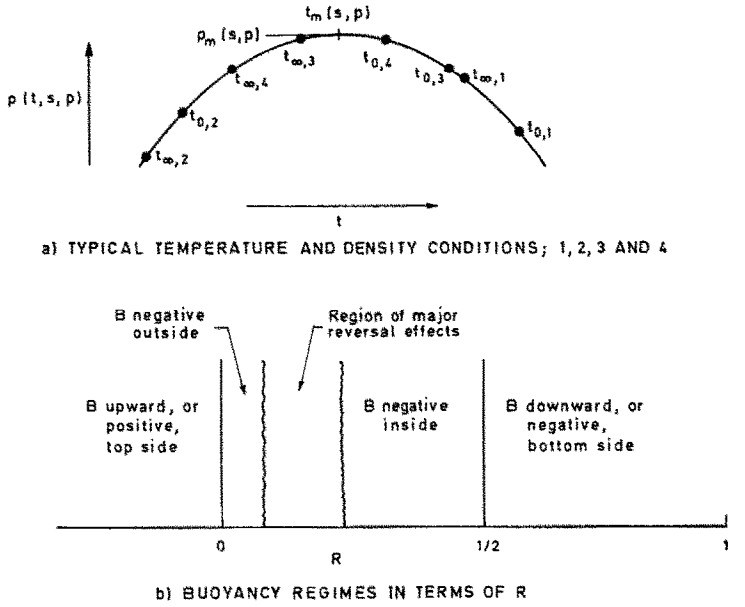

FIG. 1. Flow regime characteristics across the range of temperature conditions, t_0, t_∞ and $t_m(s,p)$, in terms of the parameter $R = [t_m(s,p) - t_\infty]/(t_0 - t_\infty)$. (a) Typical temperature and density conditions; 1, 2, 3 and 4. (b) Buoyancy regimes $B = g(\rho_\infty - \rho)$ in terms of R.

extremely important in analysis of thermally driven flows in both pure and saline water at low temperatures.

The calculations in ref. [11] used a numerical shooting method which was very sensitive to buoyancy force reversals. No solutions were obtained for these conditions. These reversals tend toward flow reversal across the boundary region. Carey *et al.* [13], refining the numerical method used in ref. [11], found additional regions of solutions in from both edges of the range $0 < R < 1/2$. However, a gap in the solutions remained, about $0.152 < R < 0.292$, for pure water and $Pr = 11.6$. The edges of the gap again arose from the tendency to flow reversal, outside reversal at the lower boundary of the gap and inside at the upper. The gap arises as the net buoyancy force decreases. These calculations indicated rapid transport parameter variations at both edges toward the gap. The shooting method was not suitable for further progress. The calculations of Wilson and Lee [14] also indicated a gap in R where no steady-state solutions, of the full equations, could be found.

El-Henawy *et al.* [15] then used a fixed interval, adaptive orthogonal collocation, computer code COLSYS, by Ascher *et al.* [16] and the multiple-shooting code, BOUNDS. See Bulirsch and Stoer [17] and Deuflhard [18]. Further solutions were found. Calculations came to the gap on both sides and sharply defined its extent. The results were ranges, in R, of multiple steady-state solutions. That is, for some values of R, there were several solutions. These solutions were often very different from each other, in terms of the flow and other transport characteristics. The gap of no solutions was reduced to $0.1518 < R < 0.2918$. The implications of some of these solutions, concerning instability and transition, are important.

Horizontal plane flows are subject to the same complexity demonstrated in Fig. 1 and discussed above. In addition, major effects are mediated by the motion pressure field which arises. Reversals of B again occur in the range $0 < R < 1/2$, for an isothermal surface. The calculations in ref. [10] for pure water, referred to above, encountered a gap, as the net buoyancy began to rapidly decrease, coming in on both sides. With the shooting method used, the residual gap was $0.080 < R < 0.301$, for pure water.

The results in the present calculations were obtained for fixed interval calculations using the code COLSYS. The calculations were made for $Pr = 10.6$, 11.6 and 12.6, for each of the extreme values of $q(s,p) = 1.897816$ and 1.58295 in the density relation in equation (2). These apply in pure water at 1 bar and to water of high salinity at high pressure. Again, the gap was narrowed, this time to $0.090836 < R < 0.20864$, for $q = 1.897816$ and $Pr = 11.6$. Multiple solutions were found at both edges of the gap. The following section sets forth the formulation of the boundary value problem, in terms of similarity variables. Then the results and conclusions are given.

FORMULATION OF HORIZONTAL BOUNDARY REGION FLOW

Since the density changes in cold water are very small, even compared to those in many other liquids, the uniform density continuity equation applies. However, the buoyancy force $B = g(\rho_\infty - \rho)$ will be

evaluated from equation (2). The horizontal and vertical force–momentum balances, the temperature and continuity equations and the boundary conditions are written below, in equations (3)–(7). The distance along the surface from its leading edge is x and y outward from the surface, in the direction in which the net buoyancy force prevails. The motion pressure p_m, the local difference in pressure from the local ambient hydrostatic, is generated by buoyancy in equation (4)

$$u\frac{\partial u}{\partial x}+v\frac{\partial u}{\partial y}=\nu\frac{\partial^2 u}{\partial y^2}-\frac{1}{\rho}\frac{\partial p_m}{\partial x} \tag{3}$$

$$0=-\frac{1}{\rho}\frac{\partial p_m}{\partial y}+\frac{g(\rho_\infty-\rho)}{\rho} \tag{4}$$

$$u\frac{\partial t}{\partial x}+v\frac{\partial t}{\partial y}=\frac{k}{\rho c_p}\frac{\partial^2 t}{\partial y^2} \tag{5}$$

$$\frac{\partial u}{\partial x}+\frac{\partial v}{\partial y}=0 \tag{6}$$

$$u(x,0)=v(x,0)=u(x,\infty)=p_m(x,\infty)=0,\quad t(x,0)=t_0 \quad \text{and} \quad t(x,\infty)=t_\infty. \tag{7}$$

These equations and boundary conditions are at the same level of boundary-layer approximations as those which arise in ordinary fluids, with the added Boussinesq approximation. However, the Grashof number, which again characterizes the flow, is defined instead in terms of the different density formulation necessary here.

The buoyancy force is determined from (2) at a given level of s and p, where $\alpha=\alpha(s,p)$, $\rho_m=\rho_m(s,p)$, $t_m=t_m(s,p)$ and $q=q(s,p)$, as

$$g(\rho_\infty-\rho)=g\alpha\rho_m(|t-t_m|^q-|t_\infty-t_m|^q). \tag{8}$$

With the usual streamfunction, the following transformation is used.

$$\eta(x,y)=b(x)y,\quad \psi(x,y)=vc(x)f(\eta) \tag{9}$$

$$\phi(\eta)=\frac{t-t_\infty}{t_0-t_\infty} \tag{10}$$

$$p_m=a(x)P(\eta). \tag{11}$$

Recalling from equation (1) that

$$R=\frac{t_m(s,p)-t_\infty}{t_0-t_\infty} \tag{1}$$

and putting (10) and (1) into (2), we evaluate the buoyancy force W

$$\rho_\infty-\rho=\alpha\rho_m|t_0-t_\infty|^q(|\phi-R|^q-|R|^q)=\alpha\rho_m|t_0-t_\infty|^q W(\eta,R). \tag{12}$$

The transformation is introduced into (3)–(7). The following similarity formulation is obtained, in terms of the stream, pressure and temperature functions f, P and ϕ. The parameters Pr, R and q arise. The primes indicate derivatives with respect to η.

$$f'''+3f''f-f'^2+\tfrac{2}{5}\eta P'-\tfrac{2}{5}P=0 \tag{13}$$

$$P'=W=|\phi-R|^q-|R|^q \tag{14}$$

$$\phi''+3Pr\phi' f=0 \tag{15}$$

$$f(0)=f'(0)=1-\phi(0)=\phi(\infty)=f'(\infty)=P(\infty)=0. \tag{16}$$

The relevant local Grashof number, the functions $a(x)$, $b(x)$ and $c(x)$ in equations (11) and (9) and the local Nusselt number are

$$Gr_x=(gx^3/\nu^2)\alpha|t_0-t_\infty|^q, \quad \text{where} \quad G=5(Gr_x/5)^{1/5} \tag{17}$$

$$a(x)=(5\nu^2\rho/x^2)(G/5)^4,\ b(x)=G/5x \quad \text{and} \quad c(x)=G \tag{18}$$

$$Nu_x=-\phi'(0)(Gr_x/5)^{1/5}. \tag{19}$$

The value of Gr_x is again the unit value gx^3/ν^2, times the nominal units of buoyancy $\alpha|t_0-t_\infty|^q$. However, this latter quantity is not a reliable indicator. This is seen as follows. The density curve in Fig. 1 applies for given values of α and q. However, for a given difference t_0-t_∞ very different density differences $\rho_\infty-\rho$ arise, depending on the location of t_0 and t_∞, in relation to t_m. Recall the regimes shown in Fig. 1(b).

The boundary-layer formulation here applies only for on-flows at a leading edge. This arises, for B positive, for flows on the upper side of a surface. For B negative, the formulation applies on the lower side.

NUMERICAL METHODS

The two-point boundary-value problem (TPBVP) in equations (13)–(16) has been solved using the Fortran code COLSYS. This is a TPBVP solver that is based upon adaptive, orthogonal collocation, using B-splines [16]. It was chosen for its accuracy, efficiency and reliability. Also, the degree of the polynomials employed in the spline approximation to solutions may be chosen to avoid potential difficulties caused by the discontinuity in the second derivative of the buoyancy force relation, W in equation (12), which arises at $\phi=R$. The computation time required was about 12–15 s per solution on a dual CPU Cyber 730 system. Compilation of the driving programs was done under FTN 4.8, Opt. = 2.

To generate families of solutions, two approaches were used. The first was simple continuation in the parameters R, beginning with a single solution found by using numerical results in ref. [10]. That solution was taken as the initial guess for a second solution with R slightly changed. Thereafter, a linear interpolation of two previous solutions was used to generate the solution for the next desired value of R. The second approach was to add the trivial equation $\dot{R}=0$ to the system of differential equations, along with

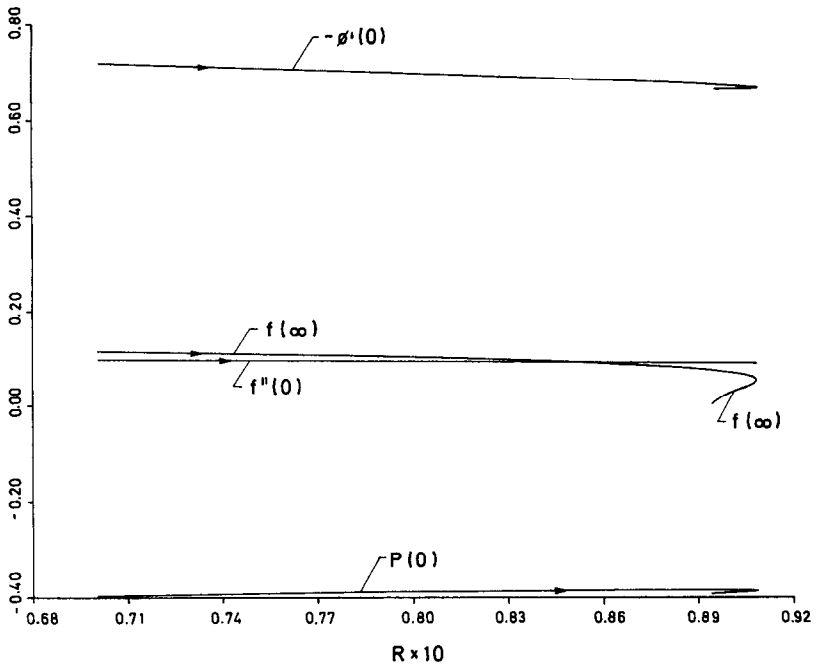

FIG. 2. Transport over the range of R just below the region of major reversal effects, up into R conditions at which multiple solutions arise. These solutions bound the gap of no known solutions from below. For an isothermal surface, $Pr = 11.6$ and $q = 1.894816$.

the boundary condition $f(\infty) = k$, when $R < 0.1$, or instead, $-\phi(0) = k$, when $R > 0.2$. Then simple continuation in k generated solutions, when the slope of a bifurcation curve of $f(\infty)$, or of $-\phi'(0)$, vs R, became large. It was sufficient to determine these solutions over the interval $(0, \eta_\infty) = 50$. To assure this, these solutions were tested, for sensitivity to η_∞, near and below the noses, that is, beyond the points of vertical tangency in bifurcation diagrams, Figs. 2 and 3. Beyond such noses lie the additional solutions. The solutions were unchanged to five significant digits for choices of $\eta_\infty = 100$ and $\eta_\infty = 150$.

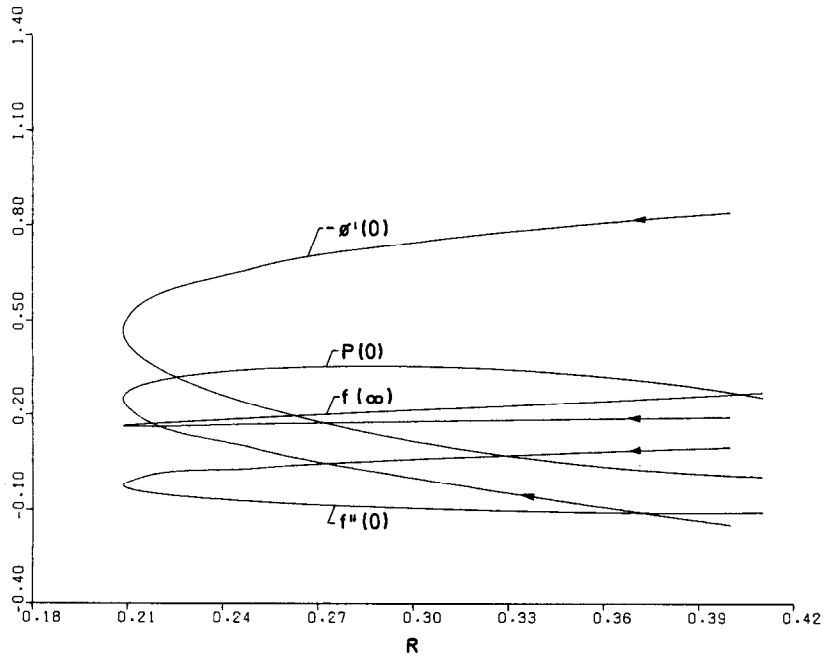

FIG. 3. Transport over the range of R just above the region of major flow reversal effects, down into R conditions at which multiple solutions arise. These solutions bound the gap of no known solutions from above. For an isothermal surface, $Pr = 11.6$ and $q = 1.894816$.

RESULTS

Solutions were obtained in the range of buoyancy force reversals, $0 < R < 1/2$. These were continued in from the two boundaries to the regions of multiple solutions. These regions bound, on the two sides, the remaining gap in which no solutions were found. Each set of solutions, those below and above the gap, were obtained for representative values of the two parameters q and R which arise in the formulation in equations (13)–(16). The values used are $q = 1.897816$ and 1.58295, for each value $Pr = 10.6$, 11.6 and 12.6. The results for each of these six conditions are given in Tables 1–6. For all q and Pr conditions the flows below the gap result from a predominantly upward buoyancy force and those above from a predominantly downward buoyancy force.

These results indicate the extent of the gap of no solutions for each of the six conditions. For $q = 1.897816$ the gap is about $0.09 < R < 0.21$ and for $q = 1.58295$ it is about $0.08 < R < 0.20$. The range of the gap is largely independent of the values of the Prandtl number, over the range 10.6–12.6. Just outside the gap, on each side, multiple solutions are found for each of the six q, Pr conditions.

The range of R over which multiple solutions are found is extremely narrow below the gap and much wider above, just as in [15]. This is seen in the tables.

Table 1. Conditions, R, and results for solutions below and above the gap, for $q = 1.894816$ and $Pr = 10.6$

R	$P(0)$	$-\phi'(0)$	$f''(0)$	$f(\infty)$
Below the gap				
0.0	−0.47260	0.79006	0.12525	0.15873
0.02	−0.45306	0.77014	0.11897	0.15094
0.04	−0.43369	0.74736	0.11244	0.14129
0.06	−0.41507	0.72066	0.10571	0.12826
0.07	−0.40640	0.70507	0.10230	0.11919
0.08	−0.39874	0.68690	0.09892	0.10602
0.09	−0.39527	0.66042	0.09587	0.069
0.090156	−0.39565	0.65924	0.09586	0.065
0.090221	−0.39618	0.65808	0.09588	0.060
0.090176	−0.39675	0.65723	0.09594	0.055
0.090053	−0.39732	0.65664	0.09602	0.05
0.089882	−0.39785	0.65626	0.09611	0.045
0.089687	−0.39835	0.65604	0.09620	0.04
0.089488	−0.39877	0.65595	0.09629	0.035
0.089300	−0.39913	0.65594	0.09636	0.03
0.088997	−0.39962	0.65609	0.09648	0.02
0.088815	−0.39983	0.65634	0.09654	0.01
0.088771	−0.39984	0.65647	0.09656	0.005
0.088755	−0.39979	0.65661	0.09655	0.0
Above the gap				
1.0	−0.76695	1.04749	0.23728	0.23978
0.8	−0.59054	0.99583	0.20108	0.29928
0.6	−0.38957	0.92721	0.15770	0.21593
0.5	−0.27616	0.88131	0.13161	0.20750
0.4	−0.14966	0.82068	0.10059	0.19712
0.3	0.00029	0.72849	0.06017	0.18347
0.21728	0.18967	0.55	−0.00020	0.16846
0.21069	0.22654	0.50	−0.01406	0.16788
0.20913	0.25830	0.45	−0.02699	0.16908
0.21193	0.28555	0.40	−0.03914	0.17201
0.21860	0.30868	0.35	−0.05066	0.17659
0.22888	0.32783	0.30	−0.06167	0.18272
0.24268	0.34288	0.25	−0.07223	0.19035
0.26019	0.35332	0.20	−0.08240	0.19952
0.28197	0.35800	0.15	−0.09218	0.21049
0.30944	0.35426	0.10	−0.10145	0.22398
0.34661	0.33429	0.05	−0.10963	0.24228

Table 2. Conditions, R, and results for solutions below and above the gap, for $q = 1.894816$ and $Pr = 11.6$

R	$P(0)$	$-\phi'(0)$	$f''(0)$	$f(\infty)$
Below the gap				
0.0	−0.46309	0.80604	0.12092	0.15416
0.01	−0.45353	0.79620	0.11792	0.15058
0.02	−0.44396	0.78569	0.11484	0.14664
0.03	−0.43444	0.77448	0.11171	0.14226
0.04	−0.42501	0.76243	0.10852	0.13733
0.05	−0.41576	0.74942	0.10528	0.13163
0.06	−0.40678	0.73518	0.10200	0.12480
0.07	−0.39830	0.71928	0.09870	0.11613
0.08	−0.39077	0.70082	0.09542	0.10368
0.084	−0.38830	0.69218	0.09414	0.09628
0.085193	−0.38768	0.68936	0.09377	0.09350
0.088217	−0.38655	0.68134	0.09286	0.08400
0.089073	−0.38645	0.67866	0.09262	0.08000
0.089423	−0.38651	0.67735	0.09254	0.07653
0.090203	−0.38670	0.67439	0.09234	0.07200
0.090643	−0.38717	0.67204	0.09226	0.06600
0.090822	−0.38778	0.67030	0.09226	0.06000
0.090836	−0.38801	0.66984	0.09227	0.05800
0.090832	−0.38824	0.66943	0.09229	0.05600
0.090822	−0.38833	0.66925	0.09230	0.05495
0.090730	−0.38894	0.66850	0.09237	0.05000
0.090464	−0.38981	0.66779	0.09251	0.04200
0.089991	−0.39086	0.66749	0.09272	0.03000
0.089724	−0.39132	0.66755	0.09282	0.02200
0.089466	−0.39167	0.66780	0.09291	0.01000
0.089423	−0.39169	0.66797	0.09292	0.00583
0.089404	−0.39170	0.66795	0.09293	0.00400
0.089391	−0.39169	0.66802	0.09293	0.00150
0.089389	−0.39169	0.66804	0.09293	0.00100
Above the gap				
1.0	−0.75093	1.0690	0.22943	0.23269
0.80	−0.57816	1.01631	0.19445	0.22249
0.60	−0.38133	0.94631	0.15254	0.20953
0.50	−0.27026	0.89952	0.12735	0.20135
0.38	−0.11944	0.82248	0.09056	0.18892
0.30	0.00044	0.74382	0.05838	0.17800
0.25	0.09440	0.66445	0.03057	0.16945
0.22	0.17482	0.57654	0.00410	0.16383
0.21	0.22542	0.50658	−0.01445	0.16282
0.20877	0.24211	0.48000	−0.02103	0.18327
0.20864	0.24806	0.47000	−0.02345	0.16358
0.20868	0.25384	0.46000	−0.02584	0.16394
0.20888	0.25945	0.45000	−0.02820	0.16436
0.20925	0.26489	0.44000	−0.03053	0.16486
0.0978	0.27018	0.43000	−0.03284	0.16541
0.21000	0.27189	0.42333	−0.03360	0.16562
0.21227	0.28510	0.40000	−0.03962	0.16746
0.22980	0.32509	0.30000	−0.06088	0.17816
0.26113	0.34936	0.20000	−0.08057	0.19458
0.30994	0.35036	0.10000	−0.09881	0.21832
0.34667	0.33137	0.05000	−0.10678	0.23607
0.38003	0.29904	0.02000	−0.10988	0.25320
0.39740	0.27530	0.01000	−0.10953	0.26304
0.41033	0.25379	0.00500	−0.10811	0.27113

Table 3. Conditions, R, and results for solutions below and above the gap, for $q = 1.894816$ and $Pr = 12.6$

R	$P(0)$	$-\phi'(0)$	$f''(0)$	$f(\infty)$
Below the gap				
0.0	−0.45456	0.82091	0.11708	0.15010
0.02	−0.43582	0.80017	0.11118	0.14281
0.04	−0.41724	0.77646	0.10504	0.13380
0.06	−0.39937	0.74869	0.09871	0.12171
0.07	−0.39105	0.73251	0.09551	0.11337
0.08	−0.38364	0.71376	0.09232	0.10151
0.09	−0.37918	0.68846	0.08933	0.07528
0.090698	−0.37941	0.68562	0.08917	0.07
0.091306	−0.38031	0.68181	0.08908	0.06
0.091357	−0.38088	0.68055	0.08911	0.055
0.091296	−0.38147	0.67964	0.08917	0.05
0.091148	−0.38205	0.67902	0.08925	0.045
0.090975	−0.38259	0.67862	0.08934	0.04
0.090575	−0.38349	0.67829	0.08951	0.03
0.090235	−0.38409	0.67834	0.08963	0.02
0.090013	−0.38440	0.67853	0.08971	0.01
0.089949	−0.38445	0.67865	0.08973	0.005
0.089915	−0.38445	0.67878	0.08974	0.0
Above the gap				
1.0	−0.73662	1.08904	0.22244	0.22640
0.8	−0.56710	1.03537	0.18855	0.21648
0.6	−0.37398	0.96411	0.14795	0.20386
0.5	−0.26500	0.91647	0.12355	0.19589
0.4	−0.14346	0.85357	0.09454	0.18608
0.3	0.00056	0.75810	0.05678	0.17316
0.26143	0.06923	0.7	0.03699	0.16686
0.22261	0.16241	0.6	0.00744	0.15980
0.21310	0.19971	0.55	−0.00561	0.15839
0.20874	0.23208	0.5	−0.01776	0.15853
0.20877	0.26018	0.45	−0.02916	0.16023
0.21265	0.28447	0.4	−0.03995	0.16345
0.23067	0.32250	0.3	−0.06012	0.17411
0.26201	0.34569	0.2	−0.07890	0.19018
0.31041	0.34672	0.1	−0.09642	0.21328
0.34674	0.32857	0.05	−0.10419	0.23055

Table 4. Conditions, R, and results for solutions below and above the gap, for $q = 1.58295$ and $Pr = 10.6$

R	$P(0)$	$-\phi'(0)$	$f''(0)$	$f(\infty)$
Below the gap				
0.0	−0.51021	0.83668	0.14091	0.17315
0.02	−0.49008	0.81187	0.13308	0.16128
0.04	−0.46953	0.78292	0.12478	0.14695
0.05	−0.45958	0.76644	0.12053	0.13785
0.06	−0.45026	0.74795	0.11625	0.12608
0.07	−0.44246	0.72585	0.11201	0.10754
0.072454	−0.44113	0.71925	0.11099	0.10
0.074609	−0.44053	0.71244	0.11013	0.09
0.075780	−0.44086	0.70758	0.10970	0.08
0.076084	−0.44125	0.70579	0.10960	0.075
0.076245	−0.44174	0.70436	0.10957	0.07
0.076288	−0.44209	0.70325	0.10958	0.065
0.076243	−0.44287	0.70243	0.10962	0.06
0.076134	−0.44344	0.70184	0.10969	0.055
0.075982	−0.44400	0.70145	0.10977	0.05
0.075631	−0.44496	0.70109	0.10994	0.04
0.075306	−0.44566	0.70110	0.11009	0.03
0.075074	−0.44606	0.70128	0.11019	0.02
0.074953	−0.44618	0.70152	0.11024	0.01
0.074933	−0.44615	0.70165	0.11025	0.005
0.074938	−0.44607	0.70179	0.11024	0.0
Above the gap				
1.0	−0.72663	1.0224	0.22317	0.23268
0.8	−0.59680	0.98826	0.19898	0.22593
0.6	−0.41972	0.93938	0.16542	0.21705
0.5	−0.30964	0.90388	0.14279	0.21120
0.4	−0.18104	0.85398	0.11380	0.20368
0.2	0.23146	0.55164	−0.00698	0.17832
0.19631	0.26868	0.50	−0.02166	0.17886
0.19694	0.29973	0.45	−0.03493	0.18094
0.20138	0.32614	0.40	−0.04736	0.18449
0.22019	0.36662	0.30	−0.07031	0.19567
0.25217	0.38966	0.20	−0.09121	0.21209
0.30160	0.38675	0.10	−0.11007	0.23544
0.33900	0.36365	0.05	−0.11798	0.25286

Only two branches, that is, two solutions were obtained above the gap, for all six conditions of q and Pr. There were also two solutions for each R just below the gap. However, for $q = 1.58295$ and $Pr = 10.6$, a third solution also arose. This effect is seen in the R column in Table 4. However, the third solution was found only over an extremely narrow range of R. For this solution, the extrainment velocity $f(\infty)$ is very low, less than 0.005.

A significant difference between the sets of solutions below and above the gap is seen, for example, in Table 1 and Fig. 3. On the figure, the direction of calculation, down from $R = 1/2$, is indicated by the arrows on the curves. That is, calculations proceeded in from $R = 1$ along the upper branch of the $-\phi'(0)$ curve shown. It is seen that as $-\phi'(0)$ continues to decrease, second solution arises at the nose. The motion pressure $P(\eta)$ increases to become positive at the surface. That is, $P(0) > 0$. The distributions of $P(\eta)$ across the boundary region, plotted in Fig. 7, show this effect. This is a result of the larger entrainment rate for these solutions, as indicated by the increasing entrainment velocity $f(\infty)$ seen in Table 1. For the weaker flows, below the gap, $P(0)$ is always negative.

As an example of the effects of buoyancy force reversals in the range $0 < R < 1/2$, on flow and multiple solutions, Figs. 2–11 are given. They are all for the particular condition $q = 1.894816$, $Pr = 11.6$. This applies for pure water at 1 atm, at low temperature levels. Figures 2 and 3 show the variation of $-\phi'(0)$, $f(\infty)$, $f''(0)$ and $P(0)$ in the regions of multiple solutions both above and below the gap. On the other hand, Figs. 4–11 show the distributions of principal transport quantities locally across the boundary region, for several values of R. These quantities are: $W(\eta)$, the buoyancy force; $\phi(\eta)$, the temperature; $\phi'(\eta)$, its slope; $f'(\eta)$, the tangential velocity component u; $f''(\eta)$, its slope; $P(\eta)$, the motion pressure; $3f(\eta) - 2\eta f'(\eta)$, the normal component of velocity v; and $f(\eta)$, the streamfunction, which becomes $f(\infty)$, the entrainment.

These distributions are shown for four representative pairs of multiple solutions, each pair at essentially the same value of R. Two pairs are below the gap, where the buoyancy force W is largely upward. They are at

Table 5. Conditions, R, and results for solutions below and above the gap, for $q = 1.58295$ and $Pr = 11.6$

R	$P(0)$	$-\phi'(0)$	$f''(0)$	$f(\infty)$
Below the gap				
0.0	−0.49986	0.85365	0.13608	0.16814
0.02	−0.48019	0.82831	0.12849	0.15700
0.04	−0.46009	0.79874	0.12045	0.14290
0.06	−0.44124	0.76308	0.11294	0.12294
0.07	−0.43354	0.74068	0.10806	0.10559
0.072069	−0.43236	0.73516	0.10723	0.10
0.074669	−0.43141	0.72722	0.10620	0.09
0.076141	−0.43154	0.72149	0.10566	0.08
0.076789	−0.43235	0.71763	0.10546	0.07
0.076893	−0.43288	0.71628	0.10544	0.065
0.076889	−0.43347	0.71525	0.10547	0.06
0.076805	−0.43406	0.71450	0.10553	0.055
0.076670	−0.43463	0.71399	0.10560	0.05
0.076325	−0.43565	0.71347	0.10577	0.04
0.075988	−0.43641	0.71339	0.10592	0.03
0.075736	−0.43687	0.71353	0.10603	0.02
0.075597	−0.43705	0.71375	0.10608	0.01
0.075568	−0.43704	0.71387	0.10610	0.005
0.075564	−0.43698	0.71400	0.10609	0.0
Above the gap				
1.0	−0.71150	1.04336	0.21576	0.22580
0.8	−0.58433	1.00855	0.19240	0.21924
0.6	−0.41088	0.95872	0.16000	0.21062
0.4	−0.17709	0.87168	0.11027	0.19764
0.2	0.22536	0.56639	0.00570	0.17294
0.19811	0.23761	0.55	−0.01028	0.17291
0.19561	0.27116	0.50	−0.02353	0.17375
0.19701	0.30018	0.45	−0.03594	0.17602
0.20190	0.32508	0.40	−0.04762	0.17967
0.20998	0.34613	0.35	−0.05871	0.18461
0.22114	0.36337	0.30	−0.06929	0.19077
0.25309	0.38528	0.20	−0.08913	0.20679
0.30296	0.38261	0.01	−0.10721	0.22947
0.33900	0.36065	0.05	−0.11493	0.24638

Table 6. Conditions, R, and results for solutions below and above the gap, for $q = 1.58295$ and $Pr = 12.6$

R	$P(0)$	$-\phi'(0)$	$f''(0)$	$f(\infty)$
Below the gap				
0.0	−0.49061	0.86946	0.13180	0.16369
0.02	−0.47134	0.84361	0.12442	0.15262
0.04	−0.45165	0.81347	0.11661	0.13928
0.06	−0.43317	0.77716	0.10858	0.12010
0.07	−0.42557	0.75445	0.10457	0.10370
0.073243	−0.42383	0.74552	0.10329	0.095
0.075621	−0.42319	0.73770	0.10240	0.085
0.077216	−0.42399	0.73015	0.10185	0.070
0.077381	−0.42451	0.72855	0.10181	0.065
0.077421	−0.42510	0.72732	0.10183	0.060
0.077368	−0.42570	0.72640	0.10187	0.055
0.077249	−0.42629	0.72576	0.10194	0.050
0.076912	−0.42737	0.72506	0.10210	0.040
0.076565	−0.42818	0.72490	0.10226	0.030
0.076296	−0.42869	0.72499	0.10237	0.020
0.076138	−0.42892	0.72519	0.10243	0.010
0.076100	−0.42893	0.72530	0.10244	0.005
0.076089	−0.42889	0.72543	0.10245	0.0
Above the gap				
1.0	−0.69797	1.06289	0.20918	0.21971
0.8	−0.57319	1.02745	0.18654	0.21332
0.6	−0.40297	0.97672	0.15517	0.20493
0.5	−0.29716	0.93990	0.13401	0.19940
0.3	−0.02316	0.80565	0.06997	0.18239
0.2	0.22003	0.57996	−0.00467	0.16818
0.19524	0.27282	0.50	−0.02500	0.16925
0.19717	0.30029	0.45	−0.03671	0.17169
0.20243	0.32389	0.40	−0.04776	0.17542
0.22204	0.36029	0.30	−0.06831	0.18641
0.25394	0.38124	0.20	−0.08724	0.20208
0.30248	0.37875	0.10	−0.10462	0.22415
0.33901	0.35776	0.05	−0.11217	0.24061

$R = 0.089423$ and 0.090822. The second value is very near the lower boundary of the gap. The two pairs above the gap, largely downward W, are at $R = 0.38$ and 0.21. The second value is near the upper boundary of the gap. The last two pairs are very far apart, compared with the pair below the gap. Both of the second values above are near the two noses of the bifurcation diagrams in Figs. 2 and 3. The two separate solutions for each of the four pairs chosen are labelled on Figs. 4–11 as u for upper branch and l for lower branch. The upper branch, on each side of the gap, are the first solutions, coming toward the gap from $R = 0$ and $R = 1/2$, respectively. This is apparent in Figs. 2 and 3. Above the gap, the upper branch solutions are more vigorous transport, at higher $-\phi'(0)$.

Figures 4–11 indicate substantial differences between the two solutions at each of the four values of R. The distribution corresponding to $R = 0.38, l$ stands out from the rest in each figure. It has the lowest $-\phi'(0)$, in Fig. 9, and most extreme maximum and minimum values of tangential and normal components of dimensionless velocity, $f'(\eta)$ and $3f(\eta) - 2\eta f'(\eta)$, in Figs. 6 and 11. In all of these figures, the four negative buoyancy force solutions, at $R = 0.21$ and $R = 0.38$, are easily distinguished from each other. They are also very different for the other solutions. However, the four solutions below the gap cannot be readily distinguished from each other at the scale at which Figures 4, 5, 7 and 9 are drawn.

The distributions of $W(\eta,R)$ vs η illustrate this difference. Those at $R = 0.21$ and $R = 0.38$, both u and l, steadily decrease to a negative minimum as η increases outward. The u and l curves in each pair have essentially the same value at their minima. The lower solutions reach their minimum nearer the surface than do the upper solutions. The curve for $R = 0.38, l$ has its negative minimum, about -0.16, at $\eta \simeq 2.8$. The distributions of $W(\eta,R)$ vs η for the other side of the gap all descend to a much larger negative minimum and rise slowly to 0 as η increases to η_∞.

The $\phi(\eta)$ distributions shown in Fig. 5 have the same qualitative behavior. They descend according to equations (15) and (16), from $\phi(0) = 1$ strictly monotonically, to 0. The results below the gap are again essentially indistinguishable from each other. The $R = 0.38, l$ curve has by far the slowest initial descent. The curve for $R = 0.38, u$ descends most rapidly.

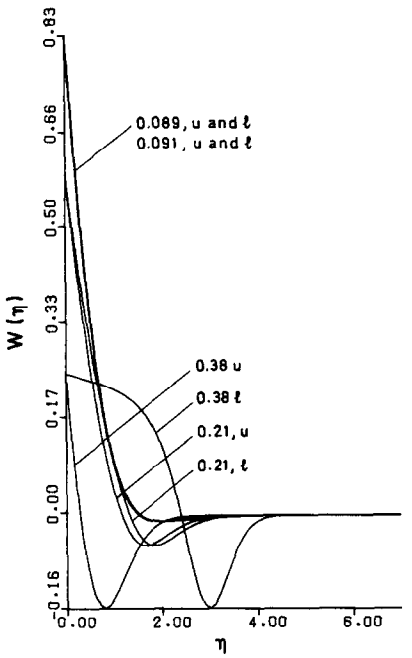

FIG. 4. The buoyancy force distribution $W(\eta)$ across the thermal boundary layer for an isothermal surface, $Pr = 11.6$, and $q = 1.894816$. In the lower and upper regions of R of multiple solutions, the upper and lower branch solutions are shown as u and l for the conditions (a)–(d) below. (a) $R = 0.089$; where $f(\infty) = 0.077$ and 0.006, essentially the same result on both branches. (b) $R = 0.091$; where $f(\infty) = 0.060$ and 0.055. (c) $R = 0.38$; where $-\phi'(0) = 0.822$ and 0.020. (d) $R = 0.21$; where $-\phi'(0) = 0.507$ and 0.423.

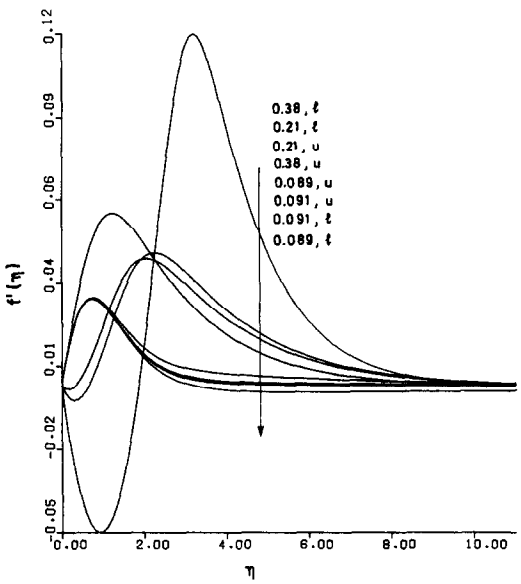

FIG. 6. The distribution of the tangential velocity component $f'(\eta)$ for the same conditions as in Fig. 4.

Some of the solutions above the gap have major reversals in the tangential velocity profiles (see Fig. 6). Most notable is the very highly bidirectional flow, for $R = 0.38,l$. This results from the very large reversal of $W(\eta)$ seen in Fig. 4. On the other hand, the solutions below the gap show, at most, slight outside reversals, for $R = 0.89423,l$ and $0.90822,l$. The outside reversals first occur at $f(\infty) = 0.05$ as $f(\infty)$ decreases from 0.8. These reversals become stronger as $f(\infty)$ decreases from 0.05 to 0. These solutions correspond

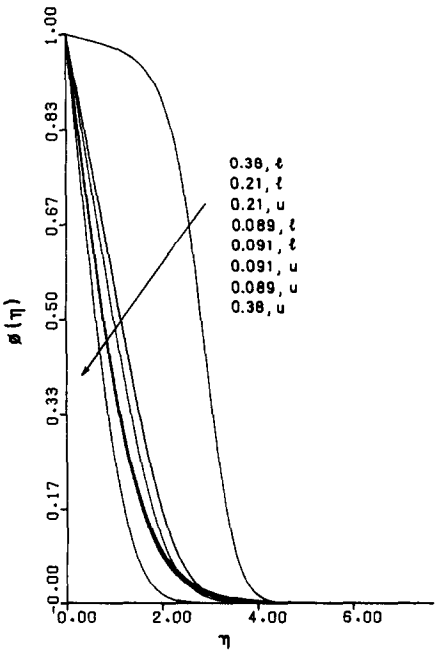

FIG. 5. The temperature distribution $\phi(\eta)$ for the same conditions as in Fig. 4. The fourth through the seventh curves are essentially the same.

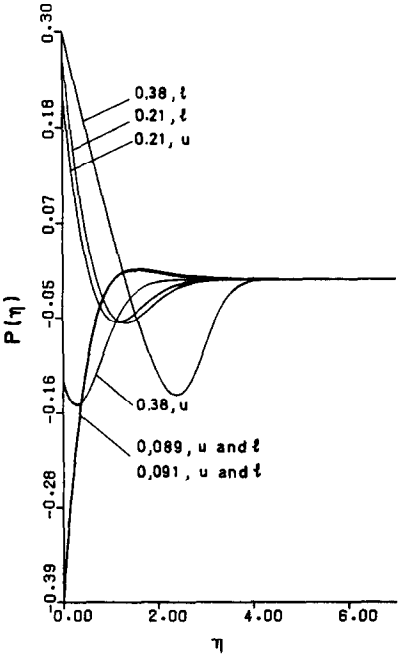

FIG. 7. The pressure distribution $P(\eta)$ for the same condition as in Fig. 4. The values for $R = 0.089$ and 0.091 are essentially the same.

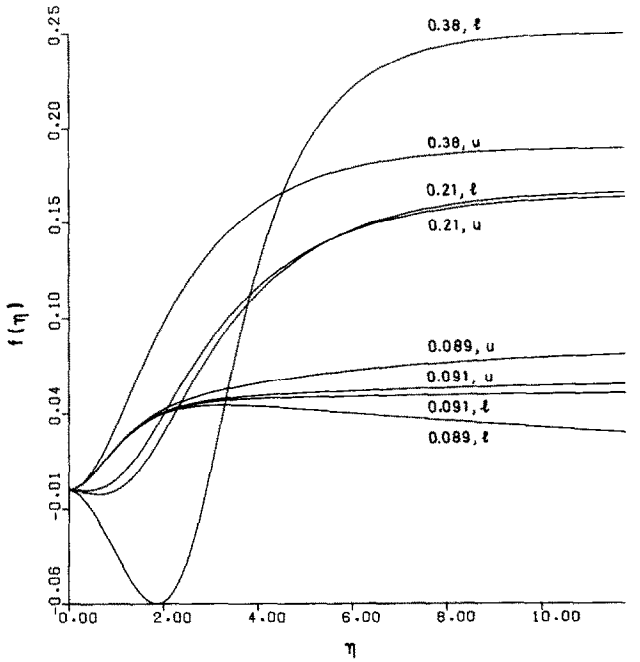

FIG. 8. The streamfunction distribution $f(\eta)$, where $f(\infty)$ is the entrainment velocity, for the same conditions as in Fig. 4.

to points below the nose of the $f(\infty)$ curve in Fig. 2. This behavior contrasts with that for flow adjacent to a vertical isothermal surface. Then the corresponding outside reversals in f' first occur for values of $f(\infty)$ above the nose in the analogous bifurcation diagram. For the solutions below the gap, $P(0)$ is always negative for all solutions. See Tables 1–6.

In the region above the gap, some but not all of the new solutions found have inside tangential velocity reversals, that is, in $f'(\eta)$. These first occur at $-\phi'(0) = 0.557$, for $R = 0.21$, as $-\phi'(0)$ decreases from 1.0690 at $R = 1.0$. These reversals arise above the nose of $-\phi'(0)$ in the bifurcation diagram, Fig. 3, just as for vertical flows, see El-Henawy *et al.* [15]. However, here these reversals occur later, that is, closer to the nose. None of the solutions found by Gebhart *et al.* [10] had inside reversals. Further, for

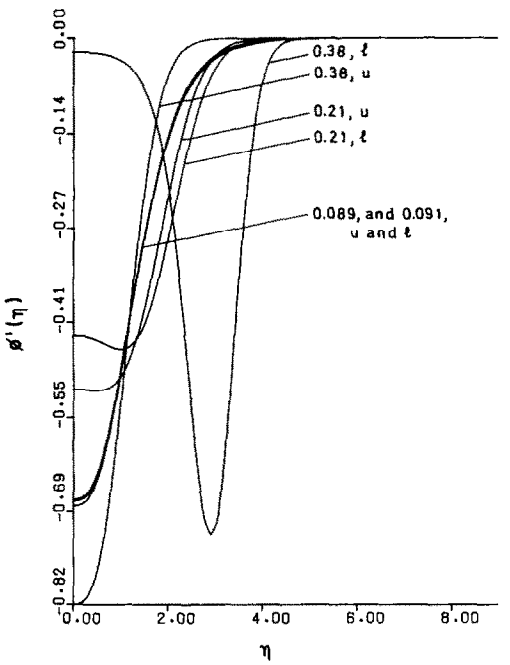

FIG. 9. The slope of the temperature distribution, $\phi'(\eta)$, for the same conditions as in Fig. 4.

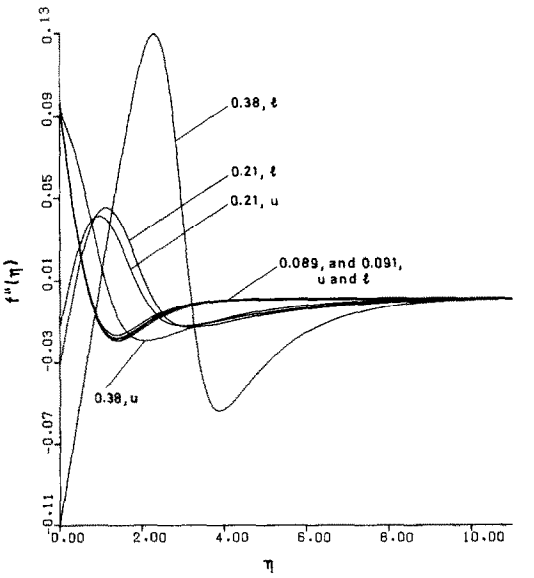

FIG. 10. The distribution of the shear stress parameter $f''(\eta)$ for the same conditions as in Fig. 4.

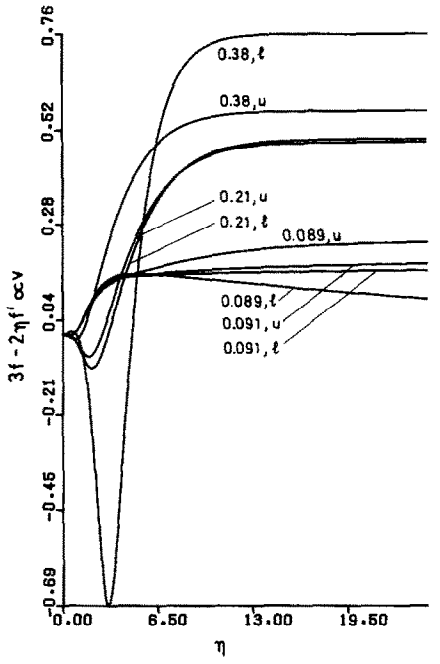

FIG. 11. The distribution of the normal component of velocity, $3f-2\eta f'$, for the same conditions as in Fig. 4.

the same value of $-\phi'(0)$ as in vertical flows, the inside reversals are stronger. For example, here, at $\phi'(0) = 0.02$ for $R = 0.38$

$$\min_{[0,\eta_\infty]} f'(\eta) = f'(0.9278) = -0.0594 \quad \text{for} \quad \eta = 50.$$

For vertical flows, for the same values of q and Pr, at $-\phi'(0) = 0.02$ for $R = 0.43060$

$$\min_{[0,\eta_\infty]} f'(\eta) = f'(0.8991) = 0.0511 \quad \text{for} \quad \eta_\infty = 100.$$

For these same solutions, for horizontal flow we have

$$\min_{[0,\eta_\infty]} f(\eta) = f(1.8194) = -0.0623$$

while for the vertical flow

$$\min_{[0,\eta_\infty]} f(\eta) = f(1.8297) = -0.0620.$$

Again considering the solutions above the gap, it is seen that, as solutions march down the bifunction curve, of $-\phi'(0)$ vs R in Fig. 3, $P(0)$ increases monotonically upward toward zero. It becomes positive slightly before $f''(0)$ changes sign. It continues to increase as $-\phi'(0)$ decreases further. Continuing calculations do result in $P(0)$ again decreasing. The distributions of $P(\eta)$ are shown in Fig. 7. For both $R = 0.21$ and 0.38, both the upper and lower solutions have reversals. Those for $R = 0.38$ are about twice those for $R = 0.21$.

The streamfunction distributions, $f(\eta)$ in Fig. 8, are all readily distinguished from each other. Again $R = 0.38,l$ stands out from the rest. It has the deepest negative minimum and the largest value of $f(\infty)$. For the gradient $-\phi'(0)$ in Fig. 9 all the curves for conditions above the gap may be distinguished from each other. The largest magnitude of $\phi'(0)$ is for $R = 0.38,u$. The smallest is for $R = 0.38,l$—a very weak flow. All of the other conditions result in intermediate values.

The distributions $f''(\eta)$ are seen in Fig. 10. The most notable one is again that for $R = 0.38,l$. There is a large negative value of $f''(0)$. This follows again from the large inside reversal of $W(\eta)$ seen in Fig. 4. That leads to the low heat transfer rate, seen as $-\phi'(0)$ in Fig. 3. A similar tendency is seen in Fig. 10, at $R = 0.21$. This effect, and the flow reversals seen in Fig. 6, would perhaps have very destabilizing effects on such flows. Multiple inflection points arise. There are also two points of inflection for the solutions below the gap, with corresponding implications of instability. That the flow reversals of f', both inside and outside, occur later for these horizontal flows, than for vertical flows, suggests that comparable horizontal flows may be more stable.

Figure 11 shows the distributions of the normal component of velocity, v, which is proportional to $3f'-2\eta f$. The very different behavior for $R = 0.38,l$ again results from the major reversals of $W(\eta)$ and of $u \propto f'(\eta)$. The large tangential flow effects generate large gradients in the cross-stream component. Some of this same effect is also seen for $R = 0.21$. The weak and more uni-directional flows below the gap do not show these characteristics.

SUMMARY

Previous calculations of horizontal flow in cold water clarified transport generally over a wide range of R. The two limiting results given in the range $0 < R < 1/2$ in ref. [10] indicate that buoyancy force reversals there soon result in diminished heat transfer and shear stress, $-\phi'(0)$ and $f''(0)$.

The above calculations examined such questions in much greater depth and detail. The gap in the solutions was significantly narrowed and its extent determined. Multiple solutions arose in the regions at each edge. Transport immediately below the gap is weak, for all solutions, because of the outside force buoyancy reversal. However, the two sets of multiple solutions above the gap have very different characteristics from each other. The buoyancy force reversal is then inside. The upper branch results show a vigorous, relatively high heat transfer rate flow. The lower branch results give much lower heat transfer. The flow then results from a more detailed inter-play of the flow, pressure and viscous effects.

The multiple solutions arise, coming in toward the gap on both sides, in conjunction with the increasingly large buoyancy force reversal across the thermal layer. Multiple responses to this reversal eventually satisfy the governing equations, in these narrow ranges. It is not now known why and how increasingly severe reversals preclude further solutions. Nevertheless, the

smooth turning back of the solution curves at both edges of the gap, in Figs. 2 and 3, strongly suggest that there are no other solutions just inside those regions.

The second solutions found for vertical flows, by El-Henawy *et al.* [15], have been analyzed for their stability by El-Henawy *et al.* [19]. All such flows were found to be unstable. This would be expected also for the lower branch solutions given here.

Acknowledgements—Ibrahim El-Henawy and Nicholas D. Kazarinoff acknowledge support for this study from the NSF Grant MCS 81 06657. Benjamin Gebhart acknowledges support from NSF Grant MEA 84 18517.

REFERENCES

1. E. Schmidt, Schlierenaufnahmen des Temperaturfeldes in der Nahe warmebgebender Körper, *Forsch. Geb. Ingwes.* **3,** 181–189 (1932).
2. K. Stewartson, On free convection from a horizontal plate, *Z. angew. Math. Phys.* **9a,** 276–281 (1958).
3. W. N. Gill, D. W. Zeh and E. del Casal, Free convection on a horizontal plate, *Z. angew. Math. Phys.* **16,** 539–541 (1965).
4. Z. Rotem and L. Claassen, Free convection boundary-layer flow over horizontal plates and discs, *Can. J. Engng* **47,** 461–468 (1969).
5. Z. Rotem and L. Claassen, Natural convection above unconfined horizontal surfaces, *J. Fluid Mech.* **38,** 173–192 (1969).
6. Z. Rotem, Contribution to the theory of free convection from horizontal plates. In *Proc. First Canadian National Congress on Applied Mechanics*, Vol. 2.
7. L. Pera and B. Gebhart, Natural convection boundary layer flow over horizontal and slightly inclined surfaces, *Int. J. Heat Mass Transfer* **16,** 1131–1146 (1973).
8. L. Pera and B. Gebhart, On the stability of natural convection boundary layer flow over horizontal and slightly inclined surfaces, *Int. J. Heat Mass Transfer* **16,** 1147–1163 (1973).
9. P. Blanc and B. Gebhart, Buoyancy induced flows adjacent to horizontal surfaces. In *Proc. Fifth Int. Heat Transfer Conference*, Tokyo, Paper No. NC1.5, pp. 20–24 (1974).
10. B. Gebhart, M. W. Bendell and H. Shaukatullah, Buoyancy-induced flows adjacent to horizontal surface in water near to density extremum, *Int. J. Heat Mass Transfer* **22,** 137–149 (1979).
11. B. Gebhart and J. C. Mollendorf, Buoyancy-induced flows in a liquid under conditions in which density extrema may arise, *J. Fluid Mech.* **89,** 673–707 (1978).
12. B. Gebhart and J. C. Mollendorf, A new density relation for pure and saline water, *Deep Sea Res.* **24,** 813–848 (1977).
13. V. P. Carey, B. Gebhart and J. Mollendorf, Buoyancy force reversals in vertical natural convection flow in cold water, *J. Fluid Mech.* **97,** 279–297 (1980).
14. N. W. Wilson and J. J. Lee, Melting of a vertical ice wall by free convection with fresh water, *Trans. Am. Soc. mech. Engrs*, Series C, *J. Heat Transfer* **103,** 13–18 (1981).
15. I. El-Henawy, B. D. Hassard, N. D. Kazarinoff, B. Gebhart and J. Mollendorf, Numerically computed multiple steady states of vertical buoyancy-induced flows in cold pure water, *J. Fluid Mech.* **122,** 235–250 (1982).
16. R. Ascher, J. Christiansen and R. D. Russell, COLSYS—a collocation code for boundary value problems. In *Codes for Boundary-Value Problems in Ordinary Differential Equations* (Edited by G. Goos and J. Hartmanis), *Lecture Notes in Computer Science*, Vol. 76, pp. 164–185. Springer-Verlag, New York (1978).
17. R. Bulirsch and J. Stoer, Numerical treatment of ordinary differential equations by extrapolation methods, *Num. Math.* **9,** 1–13 (1966).
18. R. Deuflhard, Recent advances in multiple shooting techniques. In *Computational Techniques for Ordinary Differential Equations* (Edited by Caldwell and Sayer), pp. 217–272. Academic Press, New York (1980).
19. I. El-Henawy, B. D. Hassard and N. D. Kazarinoff, A stability analysis of nontime-periodic perturbations of buoyancy induced flows in pure water near 4°C, *J. Fluid Mech.* **163,** 1–20 (1986).

SOLUTIONS PERMANENTES MULTIPLES POUR DES ECOULEMENTS HORIZONTAUX AVEC GRAVITE

Résumé—La force d'Archimède qui résulte des gradients de température dans l'eau froide est bidirectionnelle si le domaine de température couvre l'extremum de densité. Plusieurs conséquences de grande échelle ou non sont connues maintenant, pour quelques configurations parmi les plus courantes. Les premiers calculs pour les écoulements horizontaux laissent un large domaine de conditions pour lesquelles on n'obtient pas des solutions de couche limite. Des résultats présents rétrécissent considérablement ce domaine. Ils déterminent aussi avec précision le fossé résiduel sans solution en fonction d'un paramètre de densité extrémale R. Ces calculs trouvent des solutions multiples dans des domaines de R de chaque côté de ce fossé. Dans quelques régions, les propriétés du second système de solutions sont très différentes et inhabituelles, parmi les écoulements induits par gravité. De très faibles écoulements sont trouvés qui, néanmoins, peuvent être très instables. Des transferts thermiques extrêmement réduits apparaissent dans ces conditions.

MEHRFACHE STATIONÄRE LÖSUNGEN FÜR WAAGERECHTE AUFTRIEBSINDUZIERTE STRÖMUNGEN IN KALTEM WASSER

Zusammenfassung—Die Auftriebskraft aufgrund von Temperaturunterschieden im kalten Wasser kann zwei entgegengesetzte Richtungen besitzen, wenn der Temperaturbereich das Dichtemaximum einschließt. Viele Auswirkungen dieses Phänomens—im Großen wie im Kleinen—auf einige der gebräuchlichsten Strömungsanordnungen sind bekannt. Erste Berechnungen von horizontalen Strömungen zeigten, daß sich für einen weiten Bereich keine Grenzschichtlösungen ergeben. Die Ergebnisse, von denen hier berichtet wird, engen diesen Bereich erheblich ein. Sie bestimmen auch exakt das Residuum, für das keine Lösungen existieren, mit Hilfe eines Parameters R für das Dichtemaximum. Interessant ist weiter, daß Mehrfachlösungen auf beiden Seiten des Residuums gefunden wurden, und zwar über ganze Bereiche von R. In einigen Bereichen sind die Eigenschaften der Zweitlösungen sehr verschieden und ungewöhnlich für thermische Auftriebsströmungen. Sehr schwache Strömungen wurden festgestellt, die dennoch sehr instabil sein können. Unter gewissen Bedingungen wird der Wärmeübergang sehr schlecht.

МНОЖЕСТВО СТАЦИОНАРНЫХ РЕШЕНИЙ ДЛЯ ГОРИЗОНТАЛЬНЫХ ПОДЪЕМНЫХ ТЕЧЕНИЙ В ХОЛОДНОЙ ВОДЕ

Аннотация—Подъемная сила, возникающая из-за перепадов температур в холодной воде, имеет два направления в том случае, если диапазон температур включает экстремальное значение плотности. В настоящее время известно большое число масштабных и тонких следствий этого явления для некоторых наиболее известных форм течения. В первых расчетах горизонтальных течений был выявлен широкий диапазон условий, для которых решения пограничного слоя не были получены. Полученные в настоящей работе результаты значительно сужают этот диапазон. Они также точно определяют тот остаточный промежуток, в котором решения отсутствуют, через параметр экстремума плотности Я. Такой же интерес представляет тот факт, что с помощью этих расчетов обнаружено отсутствие единственности решения за пределами диапазона Я по каждую сторону промежутка. В некоторых областях свойства второго набора решений необычны и очень сильно отличаются от друяих течений, вызванных подъемной силой. Найдены очень слабые течения, которые, тем не менее, могут быть неустойчивыми. Некоторым условиям соответствуют очень малые коэффициенты теплопереноса.